CHAPTER 5

Photocatalytic Reactor Configurations for Water Purification: Experimentation and Modeling

Ajay K. Ray

Contents

1. Introduction 145
2. Macrokinetic Studies 148
   2.1 A novel kinetic reactor 152
   2.2 Distinguishing different regimes for slurry systems 154
3. Major Challenges in the Design and Development of Large-Scale Photocatalytic Reactors for Water Purification 159
   3.1 Multiple tube reactor 164
   3.2 Tube light reactor (TLR) 168
   3.3 Taylor vortex reactor 169
   3.4 Experimental details 172
4. Conclusions 181
Acknowledgments 183
References 183

1. INTRODUCTION

Wastewater treatment by low-energy UV-irradiated titanium dioxide, generally known as heterogeneous photocatalysis, has great potential as an alternative method for water purification and has become a subject of increasing interest over the last 15 years. The potential of this new technique has attracted numerous researchers to work in this area. The process couples low-energy ultraviolet light with semiconductors acting as photocatalysts. In this process, electron–hole pairs that are generated by

Department of Chemical and Biochemical Engineering, University of Western Ontario, ON N6A 5B9, Canada.
E-mail address: aray@eng.uwo.ca

Advances in Chemical Engineering, Volume 36
ISSN 0065-2377, DOI: 10.1016/S0065-2377(09)00405-0

the band-gap excitation carry out in situ degradation of toxic pollutants. The holes act as powerful oxidant to oxidize toxic organic compounds while electrons can reduce toxic metal ions to metals, which can subsequently be recovered by solvent extraction (Chen and Ray, 2001; Wang et al., 2004a, b). The first clear recognition and implementation of photocatalysis as a method of water purification was conducted by Bard (1980) and Pruden and Ollis (1983) in the photomineralization of halogenated hydrocarbon contaminants in water, including trichloroethylene, dichloromethane, chloroform, and carbon tetrachloride, sensitized by TiO_2. Since then, numerous studies have shown that a great variety of dissolved organic compounds could be oxidized to CO_2 by heterogeneous photocatalysis technique. Many reviews (Chen et al., 2000b; Fox, 1993; Hoffmann et al., 1995) and books (de Lasa et al., 2005) have also been devoted to this area of research. In the review article by Blake (1997), more than 1,200 references on the subject have been reported and an exhaustive list of chemicals that can be treated by heterogeneous photocatalysis process has also been provided.

The reason for this huge interest in photocatalysis is the significant number of advantages this process has over the traditional methods and other advanced oxidation processes of water treatment, particularly, (a) complete mineralization of many organic pollutants to environmentally benign effluents such as carbon dioxide, water, and mineral acid; (b) there is no need for use of expensive and dangerous oxidizing chemicals (such as O_3 or H_2O_2) since dissolved oxygen (or air) is sufficient; (c) TiO_2 as catalyst is active, inexpensive, nonhazardous, stable, and reusable; (d) the light required to activate the catalyst is low-energy UV-A ($\lambda < 380$ nm) of intensity around 1–5 W m^{-2} for photoexcitation, and it is also possible to use solar light as an alternative; and (e) possibility of simultaneous oxidation of toxic organics as well as reduction of toxic metals ions.

In spite of the potential of this promising technology, development of a practical water treatment system has not yet been successfully achieved. In the last decade, a large number of publications have appeared based on laboratory-scale studies with generally positive results for very diverse categories of toxic compounds in water. However, technical development to pilot-scale level has not been successfully achieved although there are numerous patents approved worldwide.

An important impediment in the development of efficient photocatalytic reactors is the establishment of effective reactor designs for large-scale use as demanded by industrial and commercial applications. In order to achieve a successful commercial implementation, several reactor design parameters must be optimized, such as the photoreactor geometry, the type of photocatalyst, and the utilization of radiated energy. In this type of reactors, besides conventional reactor complications such as reactant–catalyst contacting, flow patterns, mixing, mass transfer, reaction kinetics, catalyst installation, and temperature control, an additional engineering factor

related to illumination of catalyst becomes relevant. A fundamental issue regarding the successful implementation of photocatalytic reactors in contrast to traditional chemical reactors is the transmission of irradiation in a highly scattering and absorbing medium composed of water and fine TiO_2 particles. It is also necessary to achieve efficient exposure of the catalyst to light irradiation. Without photons of appropriate energy content, the catalyst shows no activity. The problem of photon energy absorption has to be considered regardless of reaction kinetics mechanisms. The illumination factor is of utmost importance since the amount of catalyst that can be activated determines the water treatment capacity of the reactor. The high degree of interaction between the transport processes, reaction kinetics, and light absorption leads to a strong coupling of physicochemical phenomena and no doubt, it is the major obstacle in the development of a photocatalytic reactor.

The assessment of irradiation and its distribution inside photocatalytic reactors is essential for the extrapolation of bench-scale results to large-scale operations and the comparison of the efficiencies of different installations. The successful scaling-up of photocatalytic reactors entails increasing the number of photons absorbed per unit time and per unit volume of reactor as well as efficient utilization of the electron holes created during the photocatalytic transformations. While some of the physicochemical principles of photocatalysis are relatively well understood, reactor design and reactor engineering of photocatalytic units still require consideration. Cassano et al. (1995) emphasized the importance of the selection of radiation sources and the design of reactor geometry with respect to the irradiation source including mirrors or reflectors.

The central problem in a photocatalytic reactor is focused on a uniform distribution of light to a large surface area of catalyst. For particular photoreactor geometry, scale-up in the axial and/or radial directions is constrained by the phenomenon of opacity, light scattering, depth of radiation penetration, and local volumetric light absorption. The arrangement of light source–reactor system influences the reactor design in such a strong way that independent consideration is not possible. Moreover, the need for at least one of the reactor walls to transmit the chosen radiation imposes the utilization of transparent materials, such as glass for the reactor construction, and thus imposes size limitations, sealing problems, and breakage risks.

The overall reaction rate of photocatalytic processes is usually slow compared to conventional chemical reaction rates due to low concentration level of the pollutants, and therefore, there is a need to provide large amounts of active catalyst inside the reactor. Although the effective surface area of the porous anatase catalyst coating is high, there can only be a thin coating (about 1 μm thick) applied to a surface. Thus, the amount of active catalyst in the reactor is limited, and even if individual degradation

processes can be made relatively efficient, the overall conversion efficiency will still be low. This problem severely restricts the processing capacity of the reactor, and the necessary time required to achieve high conversions are measured in hours, if not days. These aspects are discussed in detail in the section "Major challenges in the design and development of large-scale photocatalytic reactors."

The mechanism of photocatalysis reaction has been discussed in many books (de Lasa et al., 2005; Serpone and Pelizetti, 1989) and articles (Chen et al., 2000; Dutta et al., 2005). The individual steps that drive the above reaction are still not well understood due to the complex processes involved. The semiconductor photocatalytic oxidation of organic species dissolved in water by gaseous oxygen poses a number of questions with respect to the three-phase system and its interaction with light. It can, therefore, be referred to as a *four-phase* system, the fourth phase being the *UV light-electronic* phase. These questions present a great challenge, and the first step of the investigation must be a systematic study and understanding of the macrokinetic factors affecting the photocatalytic degradation rate.

2. MACROKINETIC STUDIES

TiO_2 catalyst has been used in two forms: freely suspended particles in aqueous solution and immobilized particles onto rigid inert surfaces. In the former case, a high ratio of illuminated catalyst surface area to the effective reactor volume can be achieved for a small, well-designed photocatalytic reactor (Chen and Ray, 1998), and almost no mass transfer limitation exists since the diffusional distance is very small, resulting from the use of ultrafine (<30 nm) catalyst particles. In large-scale applications, however, the catalyst particles must be filtered prior to the discharge of the treated water, even though TiO_2 is harmless to the environment. Hence, a liquid–solid separator must follow the slurry reactor (SR) (e.g., Photo-Cat® reactor of Purifics Environmental Canada Technologies). The installation and operation of such a separator will raise the cost of the overall process, as the separation of the ultrafine catalyst particles is a slow and expensive process. Besides, the penetration depth of the UV light is limited due to the strong absorption by TiO_2 and dissolved organic species, particularly for dyes. All these disadvantages render the scale-up of a SR very difficult (Mukherjee and Ray, 1999).

Many macrokinetic studies have been done to date to understand the effects of various parameters in the degradation of compounds through heterogeneous photocatalysis. The past works have analyzed various macrokinetic factors, namely (a) catalyst loading, (b) initial concentration of solute, (c) light intensity, (d) circulation rate, (e) pH of solution, (f) partial pressure of oxygen, and (g) temperature, which affect the degradation rate (Table 1). References used in Table 1 are typical references, and it should be

Table 1 Important macro kinetic factors affecting photocatalytic degradation rate as reported by few investigators in open literature

Investigators		Chen and Ray, 1998	Rideh et al., 1997	Inel and Okte, 1996	Matthews, 1990
Pollutant		4-Nitro phenol	2-Chloro phenol	Malonic acid	Phenol, 4-CP, benzoic acid
Experimental setup		Swirl-flow reactor with suspended catalyst and recirculation	Cylindrical annular Pyrex reactor with external recirculation	Annulus reactor with a pump to recirculate the suspension	Spiral reactor, with a pump to recirculate the suspension
	Macro kinetic factors	Results			
1	Initial concentration	Initial observed rate is pseudofirst-order with respect to initial concentration	Rate decreases with increase of initial concentration	Rate increases and reaches a plateau at high concentration, Langmuir-type dependence	Rate is zero-order at high concentration and first-order at low concentration
2	Catalyst loading	Rate increases and reaches a plateau at a catalyst loading of $2\,g\,L^{-1}$	Rate increases and reaches a plateau at a catalyst loading of $0.2\,g\,L^{-1}$	Rate increases and reaches a plateau at a catalyst loading of $1\,g\,L^{-1}$	At low solute concentration lowest loading gives greater rate at high solute concentration, the more the better

Table 1 (*Continued*)

	Macro kinetic factors	Results			
3	Light intensity	Rate $\propto I^{\beta}$ where β is between 0.5 and 1.0	Rate is proportional to light intensity	Rate $\propto I^{0.5}$	Not studied
4	Circulation rate	Not studied	Not studied	Rate increases with circulation rate and reaches a plateau	No significant effect of circulation rate and assumed no mass transfer limitation
5	pH	At both high and low pH values, degradation rate is quite slow, the best pH is near point of zero charge, that is, between 5.6 and 6.4	Low rate in acidic region, constant rate in neutral region and increasing rate in basic region	Rate increase with pH and reaches a plateau at pH = 9. Surface charges of TiO_2 is strongly influenced by pH	Not studied
6	Partial pressure of oxygen, P_{O_2}	Rate increases with P_{O_2} and reaches a plateau at about 0.4 atm	Rate increases nonlinearly with P_{O_2}	Not studied	Not studied
7	Temperature	Not significant	Not significant	Rate increases with T	Not studied

noted that many other authors have reported similar results but are not included here for brevity. The following general conclusions can be drawn from the past macrokinetic studies:

1. The reaction rate depends on the initial concentration of the solute. Although at high concentration, the observed rate is independent of solute concentration (zeroth-order dependence), at low concentration it shows pseudofirst-order dependence while at some intermediate concentration it follows Langmuir-type dependence (Ray and Beenackers, 1997).
2. The reaction rate increases with catalyst loading and reaches a maximum at some optimum catalyst loading and then decreases. The researchers attribute the decrease of rate at high catalyst loading to the obstruction of light transmission and defined it as the "shielding effect" (Chen et al., 2000).
3. The reaction rate is proportional to the light intensity, but at higher intensities the reaction rate becomes proportional to the square root of light intensity. It is explained that as the light intensity increase, so does the recombination rate of hole and electron (Ray and Beenackers, 1997).
4. The effect of circulation rate on the degradation rate has also been studied. Typically, no influence of circulation rate on the degradation rate has been found in slurry systems (Chen and Ray, 1998), although increases in the degradation rate due to circulation rate has been reported under some specific conditions (Inel and Okte, 1996; Serrano and de Lasa, 1997, 1999).
5. In most cases, it is found that the pH has direct impact on the degradation rate. It has been observed that the pH affects the surface properties of TiO_2 catalyst, and hence the degradation rate gets affected (Mehrotra et al., 2005).
6. The photocatalytic conversion rate increases with the increase of the oxygen partial pressure. The typical explanation is that oxygen acts as an electron scavenger, thus reducing the rate of electron–hole recombination (Chen and Ray, 1999).
7. The effect of temperature is not so significant within the studied interval, probably due to the counter effect of a decrease in the adsorption constant of solute on the catalyst with increasing thermal levels. It is also to be noted that reactions carried out in heterogeneous photocatalysis display low activation energies. Moreover, most of the photocatalytic experiments are conducted at isothermal conditions (usually at room temperature), and therefore, temperature changes do not play a major role (Chen and Ray, 1999).

One of the most important issues of macrokinetic studies is distinguishing the "kinetic" region in which the observed rate is governed by kinetic dependences. Obviously, intrinsic kinetic data are necessary for catalyst characterization and reactor design. Traditionally, in the kinetic studies of heterogeneous catalysis, to distinguish the "kinetic" regime from the

"transport-limited" regime, data related to the substance transformation over catalyst must be presented using the dependence mol per unit mass of catalyst per unit time instead of mol per unit volume of solution per unit time. This kind of data representation with dimension of rate of reaction based on per unit mass of catalyst can be found in the literature of multiphase slurry reactions with suspended catalyst. However, in the literature devoted to the photocatalytic degradation of organic solutes such representation of data is not a common feature. Typically, kinetic data are reported using the dimension mol per unit volume of solution per unit time and the "kinetic" region, rigorously to say, cannot be identified. In the next section, a novel kinetic reactor design is described that can be used for identifying different kinetic as well as transport-limited regimes for both slurry and immobilized systems. This reactor also allows determining pure kinetic rate constants and its dependence as a function of various parameters such as light intensity, amount of catalysis, pH, and oxygen concentration.

2.1. A novel kinetic reactor

Figure 1 shows a semibatch swirl-flow monolith-type reactor that has been designed to study purely the kinetics of photocatalytic reactions for any model components (Ray and Beenackers, 1997). Monoliths are unique

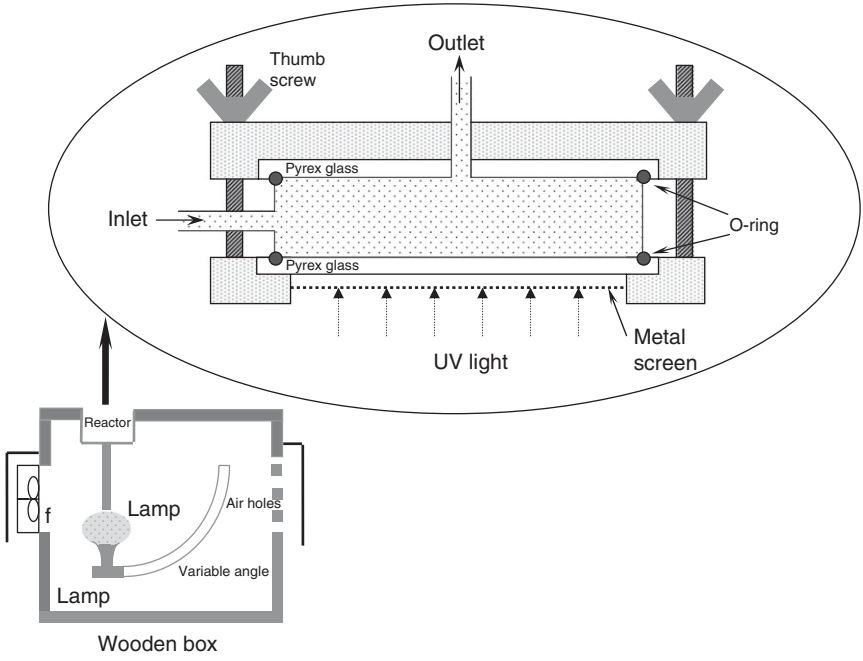

Figure 1 Schematic diagram of the novel kinetic reactor (Mehrotra et al., 2003).

catalyst supports that provide a high surface to volume ratio and allow high flow rates with low pressure drop. Catalyst has been immobilized for continuous use and to eliminate the need of separation for post-process treatment. Experiments were performed to determine the various rate constants, in particularly, the effect of light intensity and catalyst layer thickness on reaction rate constant, effect on overall reaction rate when light has to travel through the scattering and absorbing heterogeneous medium to activate the catalyst, and the effect of angle of incidence of light falling on catalyst particles. As it is apparent in most fixed-catalyst systems, mass transfer limitations do exist. However, this unique reactor can be used to determine the mass transfer effect and the correct kinetic rate constants and this to extract pure kinetic data. The reactor consists of two circular glass plates and is placed between soft padding housed within stainless steel and aluminium casing separated by 3–10 mm (Figure 1). The catalyst is (note: to use the "present" tense) consistently better deposited either on the top of the bottom plate or on the bottom of the top plate. The polluted water is introduced tangentially between the two glass plates through an inlet tube and exited from the center of the top plate through an outlet tube. The tangential introduction of liquid created a swirl-flow and thereby helped in obtaining better mixing and residence time distribution inside the reactor.

The lamp (Philips HPR 125 W high pressure mercury vapor) is placed underneath the bottom glass plate on a holder that can be moved to create different angle of incidence of light on the catalyst plate. The lamp and reactor are placed inside a wooden box painted black so that no stray light can enter into the reactor. The lamp is constantly cooled by a fan to keep the temperature down and protect the lamp from overheating. The lamp has a spectral energy distribution with a sharp peak at $\lambda = 365.5$ nm of 2.1 W and thereby the incident light intensity of our interest is 213 W m^{-2}. Provision is made for placement of several metal screens of different mesh size between the lamp and bottom glass plate to obtain variation in light intensity.

The flow pattern inside the reactor can be calculated by solving momentum equations using commercial software package, FLUENT. Figure 2 reports the particle trajectory for both one inlet and two inlets in opposite directions. The figure clearly shows that tangential introduction of fluid indeed creates swirl-flow inside the reactor. It reveals the presence of a dead zone in upper right corner and bypassing of fluid when one inlet stream is used. The location of dead zone can vary depending on the inlet velocity. In order to eliminate the dead zone and bypassing of fluid, two inlets placed in opposite directions were incorporated and the Figure 2b clearly shows improved flow patterns inside the reactor thereby resulting in uniform residence time distribution of the fluid.

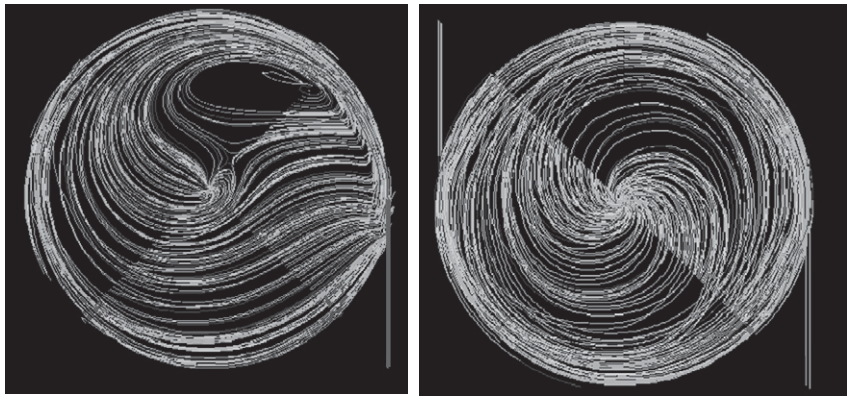

Figure 2 Flow pattern inside the reactor. (a) one inlet, (b) two inlets. Figure clearly shows use of two inlets can eliminate presence of dead volume and bypassing of fluids that is present in reactor with one inlet (Chen et al., 2001).

2.2. Distinguishing different regimes for slurry systems

Figure 3 represents experimental data of the photocatalytic degradation rate of benzoic acid for different catalyst loading while Figure 4 represents rate versus circulation rate. The experimental studies have been done with catalyst loading in the range of 0.01–2.0 g L^{-1} and at circulation rate between 50 and 1,050 mL min^{-1}. The figure reveals that the degradation rate is almost constant (independent of the catalyst loading) for catalyst loading between 0.01 and 0.05 g L^{-1}. The rate then drops gradually as the catalyst loading is increased from 0.05 to 2.0 g L^{-1}. The rate is not affected by the circulation rate at the same catalyst loading, but the magnitude of rates with respect to circulation rates is different at different catalyst loading. Clearly, Figure 3 depicts the "kinetic" regime for catalyst loading between 0.01 and 0.05 g L^{-1}. In this range, the overall rate is solely controlled by kinetics as when we double the amount of catalyst (in g-cat), the conversion (in mmol min^{-1}) also doubles, thereby the resultant rate (in mmol g^{-1}-cat min^{-1}) remains constant. When catalyst loading is increased above 0.05 g L^{-1}, the rate decreases gradually. Hence, in this region, the overall rate is not controlled entirely by kinetics and must be influenced by the transport of either pollutant or light to the catalyst surface.

In this transport-limited region, the conversion increases at a slower rate than the increase of amount of catalyst, and thereby, the overall rate decreases instead of remaining constant as in the "kinetic" regime. In other words, in this region conversion is influenced by different factors: (a) the additional catalyst surface area provided does not come in full contact with the pollutant due to external mass transfer resistance, and/or

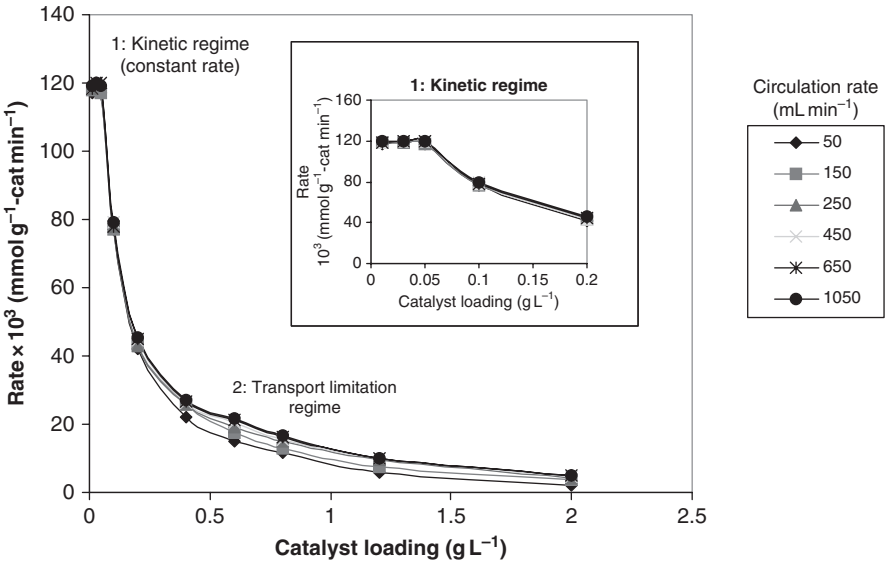

Figure 3 Degradation rate (mmol g^{-1}-cat min^{-1}) of benzoic acid for different catalyst loading showing the kinetic regime. Experimental conditions: $C_{SO} = 0.2$ mM, pH = 3.7 ~ 3.9, $T = 303$ K, $I = 9.90$ mW cm^{-2}, and O_2 saturated (Mehrotra et al., 2005).

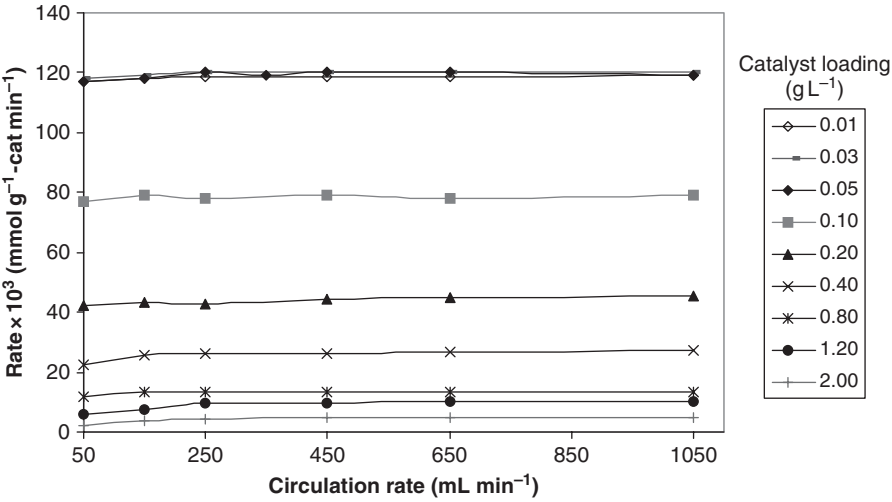

Figure 4 Degradation rate (mmol g^{-1}-cat min^{-1}) of benzoic acid against circulation rates at different catalyst loading. Experimental conditions: $C_{SO} = 0.2$ mM, pH = 3.7 ~ 3.9, $T = 303$ K, $I = 9.90$ mW cm^{-2}, and O_2 saturated (Mehrotra et al., 2005).

(b) the pollutant molecules cannot reach some of the available catalyst surface area due to agglomeration of the catalyst particles (internal mass transfer resistance), and/or (c) the irradiation provided cannot reach some catalyst surface area due to absorption and scattering (shielding effect) of light, and/or (d) the light cannot penetrate the agglomerates and activate the inner surfaces, and/or (e) there is a combination of all of the above. Thus, Figure 3 reveals two regimes: (1) "kinetic" regime at the low catalyst range ($<0.05\,g\,L^{-1}$) and (2) "transport (mass or light)" limitation regime at the high catalyst loading ($0.05\,g\,L^{-1}$–$2.0\,g\,L^{-1}$). In the transport limitation regime, the problem lies in understanding of the factor responsible for the above described transport limitations.

Figure 4 reveals that the overall reaction rate remains constant with the increase of circulation rate at any particular catalyst loading. Such results corresponding to the experimental data obtained previously (Mehrotra et al., 2005) mean that there is no external mass transfer limitation under the experimental conditions. The specific features related to our experiments are small volume of the reactor (63.5 mL), low residence time (11 s), internal stirring, and small catalyst loading (0.0125–$0.05\,g\,L^{-1}$). The difference is evident as our results clearly distinguish data related to the "kinetic" regime. In order to analyze the cause of such discrepancy in more detail, a special experiment was performed (Mehrotra et al., 2005). A beaker containing 70 mL of the slurry mixture of 0.2 mM benzoic acid and desired amount of TiO_2 catalyst was taken. The mixture was stirred in the dark for half an hour to allow for adsorption (dark reaction) of benzoic acid on the catalyst surface to reach equilibrium. The beaker was then placed over a glass plate with UV lamp underneath. The reaction mixture was bubbled with oxygen and stirred very slowly. The resultant initial rate at different catalyst loading is shown in Figure 5.

Comparing typical rate dependence on the catalyst loading from the previous studies with results reported in Figures 3 and 5, it can be concluded that at very slow internal stirring, high residence time and absence of external circulation (conditions in Figure 5) diminishes the region of rate constancy, and under certain conditions the "kinetic regime" could not be observed. Hence, proper mixing, small catalyst loading, small volume of the reactor, and low residence time, which are characteristics of our experiments shown in Figure 3, are the necessary conditions to obtain data under a well-distinguished "kinetic" regime.

To analyze the transport (mass or light) limitation regime in more detail, one can represent in Figure 6 the same experimental results of apparent rate reported in Figures 3–4 using another dimension $mmol\,L^{-1}$-solution min^{-1}, which is most commonly used in open literature by researchers working in photocatalysis. Figure 6 shows three different domains: (a) the increase of rate at the low catalyst loading, (b) the constancy of rate at the intermediate catalyst loading ("optimal catalyst loading" domain), and (c) the decrease of rate at the high catalyst loading.

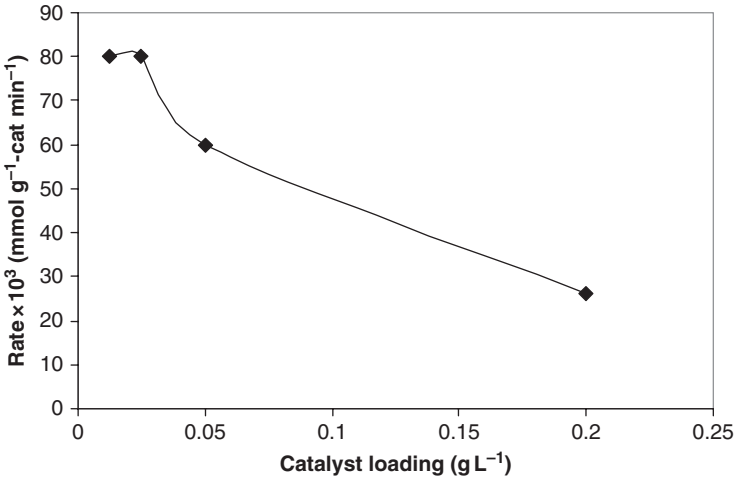

Figure 5 Degradation rate (mmol g^{-1}-cat min^{-1}) of benzoic acid for different catalyst loading without external circulation. Experimental conditions: $C_{SO} = 0.2$ mM, pH = 3.7 ~ 3.9, $T = 303$ K, $I = 8.0$ mW cm^{-2}, and O_2 saturated (Mehrotra et al., 2005).

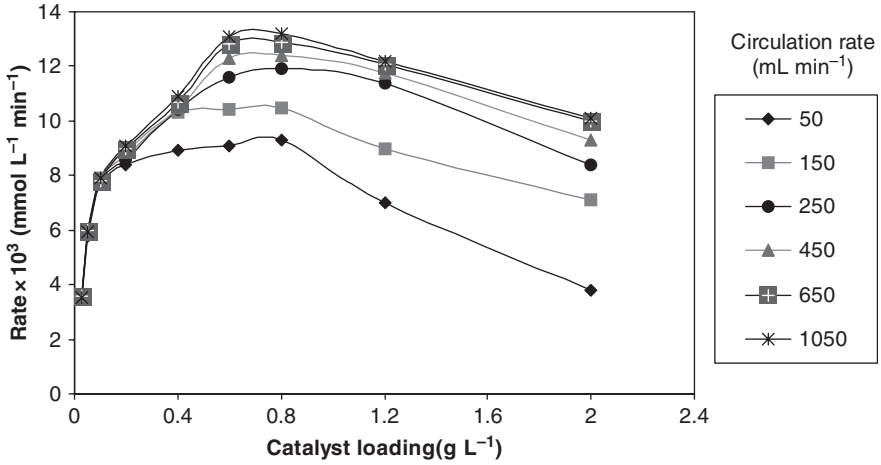

Figure 6 Degradation rate (mmol L^{-1}-solution min^{-1}) of benzoic acid against catalyst loading at different circulation rates. Experimental conditions: $C_{SO} = 0.2$ mM, pH = 3.7 ~ 3.9, $T = 303$ K, $I = 9.90$ mW cm^{-2}, and O_2 saturated (Mehrotra et al., 2005).

This plateau in the optimal loading (working regime) domain becomes smaller and even insignificant with the increase of the circulation rate. We have already reported in Figure 4 that external mass transfer is negligible as rate (in mmol g^{-1}-cat min^{-1}) was not affected by the circulation rate at any given catalyst loading. When same experimental data are plotted in

Figure 6, it shows that as the circulation rate is increased, the plateau of constant rate (in mmol L^{-1}-solution min^{-1}) not only diminishes but also shifts toward higher catalyst loading. Obviously, the circulation rate changes the transport rate, but it is not a case of the external transport limitation. It is very likely that in this region (catalyst loading between 0.4–0.85 g L^{-1}), the circulation rate influences agglomeration of catalyst particles. Internal mass transfer resistance caused by the agglomerate primarily controls the degradation rate. At higher circulation rates, the average size of agglomerated catalyst particles decreases, and therefore, the observed degradation rate increases. Another important aspect to note is the difference between pure "kinetic" regime values and values corresponding to the "optimal catalyst-loading" regime. There is a significant difference between these rates, and such difference has not been presented in the previous studies. The ratio of the rate at "optimal catalyst loading" to the rate in the "kinetic" regime can be estimated as about 0.166 irrespective of circulation rate using the dimension of rate as mmol g^{-1}-cat min^{-1} (Figure 4) for "optimal catalyst loading" of 0.8 g L^{-1} (Figure 6).

The three factors that can be considered to be responsible for the transport limitation of overall rate can be distinguished as (a) increase of catalyst loading per unit solution volume causes an increase of apparent rate, while combination of (b) mutual influence of particle (agglomeration of particles) hinders the organic substance to reach the catalyst surface, and (c) the ability of photons to penetrate agglomerates and activate the inner surfaces causes decrease of apparent rate. The first and the last two factors compensate each other in the second region (domain), resulting in a region of "optimal catalyst loading." When catalyst loading is increased further, the third factor dominates, thus reducing the apparent rate, which Figure 6 clearly demonstrates.

A sound explanation for the optimal catalyst-loading regime is the appearance of particle agglomerates under some sufficient catalyst loading. Generally, the limitation domain can be interpreted as the internal diffusion region in which the agglomerate plays the role of the porous particle. An estimation of such agglomerate size can be easily done using the known theoretical relationship for the Thiele modulus, according to which the effectiveness factor η is given by the following equation:

$$\eta = \frac{3}{R}\sqrt{\frac{D_e}{k\rho_p S_a}} \tag{1}$$

where k is the kinetic constant, D_e is the diffusion coefficient, and R is the radius of the agglomerate. The value of kinetic rate constant can be obtained using the rate value in the "kinetic" regime $\approx 4 \times 10^{-3}$ mmol L^{-1}-solution min^{-1} (Figure 6) with initial concentration, $C_{SO} = 0.2$ mmol L-solution, and specific surface area of the reactor as 100 $m^2\,m^{-3}$. Using the above values,

the degradation rate constant k for benzoic acid is equal to $3.33 \times 10^{-6}\,\mathrm{m\,s^{-1}}$. In the "optimal catalyst-loading" domain, $\eta = 0.166$, $D_e = 1 \times 10^{-10}\,\mathrm{m^2\,s^{-1}}$ (Chen et al., 2000), $\rho_p = 2.4\,\mathrm{g\,cm^{-3}}$, and $S_a = 50\,\mathrm{m^2\ g^{-1}}$, therefore, the characteristic size of the agglomerate, R, is given by

$$R = \frac{3}{\eta}\sqrt{\frac{D_e}{k\rho_p S_a}} = 9\ \mu\mathrm{m} \tag{2}$$

The agglomerate size is in close agreement with data obtained independently and reported elsewhere (Hoffmann et al., 1995) compared to average primary particle size of Degussa P25 as 30 nm.

When the catalyst loading is increased even further (greater than $1.2\,\mathrm{g\,L^{-1}}$), the overall rate is limited primarily by limitation of transport of light to the catalyst surface, which is described in literature as shielding effect. In this region, addition of more catalyst is like adding inert materials and therefore, meaningless. The most important point to note is that constancy of rate while expressing rate data as mol/mass of catalyst/time reveals the "kinetic" region whereas constancy of rate data when rate is expressed as mol/liter of solution/time reveals the region of "optimal catalyst loading." Determination of all the three regions is important, and it is possible to accomplish by representing same set of experimental data in two different rate dimensions. Intrinsic kinetics can be obtained from the "kinetic" region, which is necessary for catalyst characterization and reactor design. "Optimal catalyst loading" region is essential from a practical application point of view while the shielding region states that there is no point of adding any more semiconductor particles, which acts as an inert instead of acting as a photocatalyst.

3. MAJOR CHALLENGES IN THE DESIGN AND DEVELOPMENT OF LARGE-SCALE PHOTOCATALYTIC REACTORS FOR WATER PURIFICATION

Photocatalytic reactions are promoted by solid photocatalyst particles that usually constitute the discrete phase distributed within a continuous fluid phase in the reactor. Therefore, at least two phases, that is, liquid and solid, are present in the reactor. The solid phase could be dispersed (SPD) or stationary (SPS) within the reactor. SPD photoreactors may be operated with the catalyst particles and the fluid phase(s) agitated by mechanical or other means. Depending on the means of agitation, the photoreactor resembles that of slurry or fluidized bed reactors. In numerous investigations, an aqueous suspension of the catalyst particles in immersion or annular-type photoreactors has been used. However, the use of suspensions requires the

separation and recycling of the ultrafine (submicron size) catalyst from the treated liquid and can be an inconvenient, time-consuming expensive process. In addition, the depth of penetration of UV light is limited because of strong absorption by both catalyst particles and dissolved organic species. Above problems could be avoided in SPS photoreactors in which photocatalyst particles are immobilized onto a fixed transparent surface, such as the reactor wall or a fiber mesh, or supported on particles, such as glass or ceramic beads, that are held in fixed positions in the photoreactor. However, immobilization of catalyst on a support generates a unique problem. The reaction occurs at the liquid–solid interface and usually only a part of the catalyst is in contact with the reactant. Hence, the overall rate may be limited to mass transport of the pollutant to the catalyst surface. In addition, the rate of reaction is usually slow because of the low concentration level of the pollutant, and therefore, there is a need for a reactor whose design provides a high ratio of illuminated immobilized catalyst to illuminated surface and provides the possibility of total reactor illumination.

The volume of photocatalytic reactor can be expressed as

$$V_R = \frac{Q\, C_{\text{in}}\, X}{\kappa\, \Re} \tag{3}$$

where Q is the volumetric flow rate ($m^3\,s^{-1}$), C_{in} is the inlet pollutant concentration ($mol\,m^{-3}$), X is the fractional conversion desired, κ is illuminated catalyst surface area in contact with reaction liquid inside the reactor volume ($m^2\,m^{-3}$), and $\Re$ is the average mass destruction rate ($mol\,m^{-2}\,s^{-1}$). Hence, smallest reactor volume will result when κ and $\Re$ are as large as possible for specified values of Q, C_{in}, and X. $\Re$ is a *reaction-specific* parameter as it expresses the performance of catalyst for the breakdown of a specific model component, while κ is a *reactor-specific* parameter representing the amount of catalyst inside a reactor that is sufficiently illuminated so that it is active and is in contact with the reaction liquid. An increase in $\Re$ can be accomplished by modifying the physical nature of the catalyst in terms of its structure and morphology or by the addition of additional oxidizing agents (thereby increasing active hydroxyl radical concentrations) or band-engineering of the catalyst in which photocatalyst is chemically modified to reduce band gap and increasing catalyst activity (Zhou et al., 2006a, b, 2007a, b). Improving the breakdown rates would lead to the need of a less demanding amount of catalyst to be illuminated, and therefore, a smaller reactor volume. The parameter κ, namely illuminated specific surface area, helps to compare design efficiency of different photocatalytic reactors as it defines the efficacy to install as much active catalyst per unit volume of reaction liquid in the reactor.

One major barrier to the development of a photocatalytic reactor is that the reaction rate is usually slow compared to conventional chemical reaction rates, due to low concentration levels of the pollutants. Other crucial hurdle

is the need to provide large amounts of active catalyst inside the reactor. Even though the effective surface area of the porous catalyst coating may be high, there can only be a thin coating (about 1 μm thick) applied to a surface. Thus, even if individual degradation processes can be made relatively efficient, the overall conversion efficiency will still be low. This problem severely restricts the processing capacity of the reactor, and the time required to achieve high conversions are measured in hours, if not days.

A number of photocatalytic reactors have been patented in recent years but none has so far been developed to pilot-scale level. Based on the manner in which catalyst is used, and the arrangement of the light source and reactor vessel, all photocatalytic reactor configurations fall under four categories. They are *slurry type* in which catalyst particles are in suspension form (Chen and Ray, 1999), *immersion* type with lamp(s) immersed within the reactor (Ray and Beenackers, 1996), *external* type with lamps outside the reactor (Assink et al., 1993), and *distributive* type with the light distributed from the source to the reactor by optical means such as reflectors and light conductors (Ray, 1999) or optical fibers (Peill and Hoffman, 1995). Majority of reactors patented are variation of the SR, and classical annular reactor (CAR) of immersion or external type in which catalyst is immobilized on reactor wall (Sato, 1992; Taoda, 1993), on pipes internally (Matthews, 1990a), on ceramic membranes (Anderson et al., 1991), on glass wool matrix between plates (Cooper, 1989), on semipermeable membranes embedded (Miano and Borgarello, 1991; Oonada, 1994) in water permeable capsules (Hosokawa and Yukimitsu, 1998), on a mesh of fiberglass (Henderson and Robertson, 1989), on beads (Heller and Brock, 1993), on fused silica glass fibers (Hofstadler et al., 1994), on porous filter pipes (Haneda, 1992), on glass fiber cloth (Masuda et al., 1994), and so on. The reactors are either helical (Ritchie, 1991), spiral (Matthews, 1988), shallow cross flow basins (Cooper and Ratcliff, 1991), or optical fiber (Wake and Matsunaga, 1994). However, all these reactor designs are limited to small scales by the low values of illuminated catalyst density. The only way to apply these systems for large-scale applications is by using large numbers of multiple units.

The parameter κ (Ray and Beenackers, 1998a), namely illuminated specific surface area, helps to compare design efficiency of different photocatalytic reactors as it defines the efficacy to install as much active catalyst per unit volume of reaction liquid in the reactor. The parameter κ represents the amount of catalyst inside a reactor that is sufficiently illuminated so that it is active and is in contact with the reaction liquid. Table 2 lists κ values for the four different classes of photocatalytic reactors. In a SR, small catalyst particles could provide large surface area for reaction but essentially most of the catalyst surface area will be inactive, particularly for large reactor dimensions as the catalyst particles will not receive enough light from the external light source. This happens since the organics and the liquid medium itself are absorbing light. This is especially true for large reactor

Table 2 Comparison of κ ($m^2\ m^{-3}$) for different reactors

Photocatalytic reactor	κ (m^2/m^3)	Parameters	κ (m^{-1})	Remarks
Slurry reactor [19]	$\left[\frac{6C_c}{\rho_c}\right]\frac{1}{d_p}$	$d_p = 0.3\,\mu m$ $C_c = 0.5\,kg\ m^{-3}$	2,631[a]	Scale-up not possible
External type – annular reactor [21]	$\frac{4d_0}{d_0^2 - d_i^2}$	$d_0 = 0.2\ m$ $d_i = 0.1\,m$	27	Scale-up not possible
Immersion type – with classical lamps [16]	$\left[\frac{4\varepsilon}{1-\varepsilon}\right]\frac{1}{d_0}$	$d_0 = 0.09\,m$ $\varepsilon = 0.75$	133	Scale-up possible but large V_R
Immersion type – with novel lamps [18]	$\left[\frac{4\varepsilon}{1-\varepsilon}\right]\frac{1}{d_0}$	$d_0 = 0.0045\,m$ $\varepsilon = 0.75$	2,667	Scale-up possible with small V_R
Distributive type – with hollow tubes [22]	$\left[\frac{4\varepsilon}{1-\varepsilon}\right]\frac{1}{d_0}$	$d_0 = 0.006$ $\varepsilon = 0.75$	2,000	Scale-up possible with small V_R

[a]The value will be much lower than 2,631 m^{-1} as all the suspended catalyst particles will not be effectively illuminated. Catalyst concentration, $C_c = 0.5\,kg\ m^{-3}$, is normally used.
$\rho_c = 3800\,kg\,m^{-3}$.

dimensions, resulting in low efficiencies and the drawback of impossibility for scale-up to commercial use applications. In addition, use of suspension requires separation and recycling of the ultrafine catalyst from the treated effluent by filtration, centrifugation or coagulation, and flocculation. These add various levels of complexity to an overall treatment process and clearly decrease the economical viability of the SRs. An external-type reactor will always be limited by low values of κ. An immersion-type reactor could be scaled-up to any dimension but when classical lamps of diameter between 0.07 and 0.1 m are used, the κ value is very low even if it is assumed that the lamps occupy 75% of the reactor volume.

Many other new *innovative* type of reactor designs exist in literature, addressing specific problems and applications or others being designed especially for treating specific types of pollutants. These are in the form of treatment agents containing novalak resins, photoelectrochemistry or electrophotographic methods, use of magnetic or sound waves, photocatalysis and acoustics, catalyst particles coated with polymers as well as ion exchange process (Mukherjee and Ray, 1999). Others include the use of optical fibers as the source of illumination catalyst contained in removable filter units and water-permeable capsules containing the catalyst. Although, innovative in approach, the main problem associated with all these reactor configurations is again the issue of scale-up for commercial use purposes.

Of particular interests are several Photo-CREC-Water photocatalytic reactors developed by Professor de Lasa's research group. Their devices involve unique designs with respect to both suspended and supported catalyst. The Photo-CREC Water I reactor is an annular reactor with a lamp placed at the reactor centerline. The arrangement allows high catalyst loading of the glass mesh, good catalyst irradiation, and uniform contact of the catalyst with the circulating water. The Photo-CREC-Water I reactor was originally proposed by de Lasa and Valladares (1997). Subsequently, modifications were introduced to the original design by Serrano and de Lasa (1997). The Photo-CREC-Water II (Salaices et al., 2001) is an annular vessel with a lamp placed in the center of the reactor. In the upper section, there is a slurry distribution system ensuring intense mixing of the slurry suspension at the reactor entry. The unit is equipped with quartz windows and accessory collimator tubes. This configuration allows the measurement of photon absorption and the quantification of back and forward reflection, and it is of particular value to establish energy and quantum efficiencies in photocatalytic reactor units. Their Photo-CREC-Water III is an annular vessel with external illumination designed to simulate a solar-irradiated reactor. The reactor is irradiated externally by a set of eight UV lamps. They measured the radiation field distribution using a fiber optic sensor placed inside a concentric inner tube with the sensor device connected to a spectrophotoradiometer. The external illumination permitted the simulation of solar

irradiation, whereas the combination of internal and external illumination allowed the smoothing of the radiation field radial distribution and the increase of irradiation efficiency.

The scale-up has been severely limited by the fact that reactor configurations have not been able to address the three most important parameters, namely, light distribution inside the reactor through the absorbing and scattering liquid to the catalyst, providing high surface areas for catalyst coating per unit volume of reactor, and mixing inside the reactor (Ray and Beenackers, 1996). The new reactor design concepts must provide a high ratio of activated immobilized catalyst to illuminated surface and must have a high density of active catalyst in contact with the liquid to be treated inside the reactor. Few new design of photocatalytic reactors, addressing the above issues have been developed by our research group and are described in the next few sections.

3.1. Multiple tube reactor

In order to overcome some of these deficiencies inherent in conventional photocatalytic reactor designs, a distributive-type photocatalytic reactor design in which catalyst is fixed to a structure in the form of glass slabs (plates), rods, or tubes inside the reactor has the greatest potential for scale-up. This will allow for high values of κ and will eliminate light passage through the reaction liquid. This is advantageous because when light approaches the catalyst through the bulk liquid phase, some radiation is lost due to absorption in the liquid. In particular, this effect is more pronounced for highly colored dye pollutants as they are strong UV absorber and will therefore significantly screen the TiO_2 from receiving UV light.

Our research group considered scale-up configurations that contain both high surface areas to volume and efficient light distribution to the catalyst phase. Two ways above deficiencies inherent in conventional photocatalytic reactor designs can be overcome. First, by using a distributive type of photocatalytic reactor design in which catalyst is fixed to a structure in the form of hollow glass tubes, and second, by using an immersion-type reactor with very narrow diameter tube lamps. The design based on hollow glass tubes allows for a much higher illuminated surface area per unit reactor volume, while the other design provides not only much higher values for active catalyst surface area but also the catalyst can be activated uniformly at its highest possible level. Furthermore, the designs of the reactors are flexible enough to be scaled-up for commercial scale applications.

The limitation to the size of the reactor with light conductors is the UV transparency of the material and the light distribution to the catalyst particle. The critical and probably the most intricate factor is the distribution of the available light in the conductors to the catalyst particles and to ensure that each particle receives at least the minimum amount of light necessary

for activation. The reactor configuration conceptually applicable for photocatalysis, satisfying most of the above-mentioned requirements, is a rectangular vessel in which light conductors as glass slabs (or rods) coated on its outside surface with catalysts are embedded vertically. The lamps together with reflectors are placed on two sides of the reactor while liquid enters and exits from the other two sides. Light rays entering the conductor through one end are repeatedly reflected internally down the length and at each reflection come in contact with the catalyst present around the outer surface of the conductors. Thus, conducting materials might be considered as a means of light carrier to the catalyst. Since the ratio of the surface area on which catalyst is present to the light entering area could be as high as 500, evidently a very large catalyst area can be illuminated. Moreover, with a large number of such light conducting material packed inside the reactor, the configuration provides a high total light transfer area and allows for a higher illuminated catalyst area per unit reactor volume. Densely packing the reactor with light conducting object not only increases surface to volume ratio but also reduces the effective mass transfer diffusion length for the pollutant to catalyst surface.

The vital issue in the distributive type of reactor concept is how to introduce light from the external source efficiently into the light conductors, and likewise, how to get it out again at the proper location and in the apropos amount. The predominant obstacle we came across in the use of glass slabs (or rods) as the light-conducting object is the occurrence of total internal reflection. It transpires when light travels from denser to rarer medium and is determined by the critical angle given by

$$\theta_c = \sin^{-1}\left[\frac{n_2}{n_1}\right] \tag{4}$$

where n_1 and n_2 are the refractive indices of the denser and rarer medium, respectively. In the case of light travelling from air, to glass to air (or water), the angle θ will always exceed the critical angle, θ_c, for the interface between glass and air (or water) irrespective of angle of incidence, α (0–90°). In other words, all the light rays that are entering through the top surface will experience the phenomena of total internal reflection and will come out axially rather than emerging from the lateral surface. However, refractive index of TiO_2 (between 2.4 and 2.8) is higher than that of glass (about 1.5) in the wavelength range of 200–400 nm, and it is likely that total internal reflection would not take place when the glass surface is coated with titania. Nevertheless, if coating consists of small spheres of catalyst particles dispersed along the surface, the actual glass–titania interface will be small, as most of the glass surface will still be in contact with water. Therefore, it is best, if possible, to avoid the occurrence of total internal reflection entirely.

One way of avoiding total internal reflection is by surface roughening. Moreover, surface roughening assists in achieving better catalyst adhesion to the substrate. Both are indeed found out to be the case experimentally by us. In fact, when lateral surface was roughened by sand blasting, most of the light emerged within few centimeters and hardly any light remained thereafter in the axial direction. This is not only because roughening desists total internal reflection phenomena but also UV transparency of most light conducting material is very poor. Although the use of quartz as light conductors will naturally help to overcome light transmission problem, it will certainly make the overall reactor set-up more expensive.

The total internal reflection problem can also be effectively avoided when the surface's light that has to pass through is parallel instead of perpendicular. One such configuration is a hollow glass tube coated on its surface with semiconductor catalysts. The hollow tube might be considered as a pore carrying light to the catalyst. In this novel configuration, light rays entering through one end of the hollow tube are repeatedly internally reflected down the length of the tube and at each reflection come in contact with the annular catalyst coating present around the outer surface of the tube. Although total internal reflection could be avoided completely in this configuration, the angle of incidence of light will be a critical factor. When light falls on the glass surface, a part of it is reflected and the rest is transmitted. The ratio between the reflection and transmission of light is a strong function of angle of incidence. When the light beam is nearly parallel with the surface (α close to 0°), most of the light is reflected and exits axially rather than laterally while for light rays with α close to 90° most of the light will emerge laterally within few centimeters and barely any light will remain thereafter as reflection is only 4% for a glass–air interface. Hence, it is important that in the design of reactor based on hollow tubes, light must be guided into the conductors at a very precise angle through a combination of optical lenses and reflectors.

Computer simulation of the reactor was performed using a commercial CFD package FLUENT/UNS to determine effects of flow rates, diffusion coefficients, reaction rate constants and inlet species concentrations and intertube spacing. Application of CFD to reactors entails a number of tasks: (a) formulating the relevant transport equations, (b) establishing the necessary constitutive and closure equations, (c) formulating appropriate boundary conditions, (d) selecting the most suitable numerical techniques to solve the equations, (e) choosing (or developing) a suitable computer code to implement the numerical techniques, and (f) developing effective flow simulation strategies. In order to get accurate results, the 3D model of the reactor was divided into control volumes ranging from 120,000 to 600,000 cells distributed unevenly in the computational domain. Computation of each problem is very time consuming, as it requires at least 2,000 iterations to be performed to obtain accurate results. In the wake of this, a state-of-the-art

computational technique, viz., distributed computing, was used to expedite the calculation and overcoming the memory bottleneck present in single workstations (Periyathamby and Ray, 1999). Initially, a reasonably converged solution was obtained for the velocity and pressure equations. The reaction part of the solver was then activated, and using the almost converged solution as the initial condition, a complete solution of the reacting flow model was obtained. The converged velocity profiles at various regions of the reactor were observed to determine the degree of mixing. Fluid mixing is one of the important criteria in efficient photocatalytic reactor design as the transport of reactants from the bulk of the liquid to the catalyst surface determines the extent of fluid-catalyst contacting and overall conversion.

In Figure 7, streaklines are used to show the mixing pattern in the reactor. The streakline pattern shows that maximum mixing takes place at the bottom of the reactor where fluid enters the reactor tangentially with a swirling motion. There is also a good degree of mixing just before the fluid exits at the top of the reactor. However, the flow is uniform without much mixing in the midregion between the inlets and the outlets.

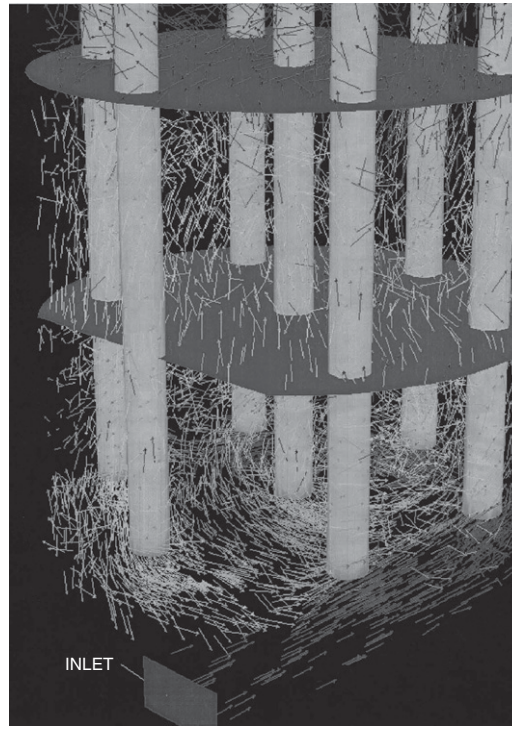

Figure 7 Velocity vectors showing the degree of mixing inside the reactor.

The advantage of using computer simulations is that the length of the reactor required for complete degradation of a particular pollutant can be determined easily compared to time-consuming expensive experimental studies. In addition, the flexibility of determining the effects of various process parameters in computer simulations will be useful, particularly flow rates, as the degradation rate strongly depends on the residence time of the fluid inside the reactor. A typical case of degradation of a pollutant, monochlorobenzene, C_6H_5Cl, is shown in Figure 8.

3.2. Tube light reactor (TLR)

During the development of this new concept of photocatalytic reactor based on multiple hollow tubes [multiple tube reactor (MTR)], we developed a unique new lamp design. These are extremely narrow diameter fluorescent tube lamps of low wattage emitting lights in the wavelength of our interest ($\lambda < 365\,nm$). These new lamps address many of the solutions to the

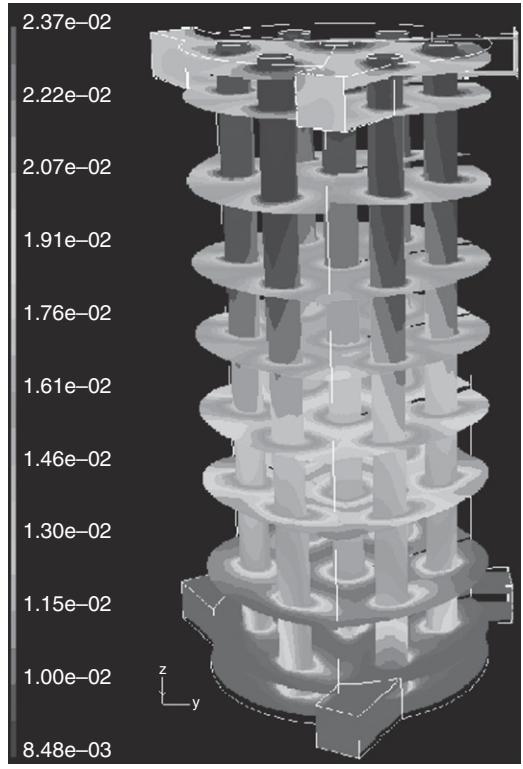

Figure 8 Photocatalytic degradation of monochlobenzene in MTR. The flow direction from bottom to top (Periyathamby and Ray, 1999).

problems that have restricted the development of technical scale photocatalytic reactors for water purification. These lamps are available in various shapes and lengths and can be placed inside a reactor to form a variety of different configurations. Development of a reactor using these new lamps will provide all the advantages of the MTRs, plus the additional advantage that catalyst could be activated at its highest level. In the reactor, catalyst was deposited on the outer surface of the low wattage lamps using a dip-coating apparatus. Thus, the main problem encountered in the development of a reactor based on multiple hollow tubes (MTR) was avoided. In the MTR concept, it is impossible to obtain a uniform light distribution along the length of the tubes and therefore, it will severely restrict the maximum length of tubes that can be used inside a reactor and thereby the overall performance of the reactor. The new lamps eliminated this drawback in the development of the MTR reactor concept, as the new design is capable of uniform light distribution over long tube lengths. Of course, this was possible with classical lamps too. However, the new lamps allow for a 50–100 times larger surface area for catalyst per unit reactor volume compared to a classical reactor design.

3.3. Taylor vortex reactor

In the design of fixed bed photocatalytic reactors, one must address two issues, namely, uniform distribution of light and mass transfer of pollutants to the catalytic surface. Earlier, our research group did experimental studies on reactors containing catalyst-coated tube bundles (Ray, 1999), catalyst-coated extremely narrow diameter immersion-type lamps (Ray and Beenackers, 1998), and catalyst-coated rotating tube bundles (Ray, 1998). The experimental as well as simulation results revealed that photocatalytic reaction is primarily diffusion (mass transfer) controlled when catalyst is fixed (Periyathamby and Ray, 1999). The photocatalytic reaction takes place at the fluid-catalyst interface, and in most cases, the overall rate of reaction is limited to the transfer of pollutants to the catalyst surface. In our earlier studies, we have enhanced mass transfer by increasing mixing through turbulence and/or use of baffles. This new reactor design uses flow instability to increase reaction yield throughout the reactor volume. We considered unsteady Taylor–Couette flow in between two coaxial cylinders where inner cylinder coated with TiO_2 catalyst is rotated at different speed to achieve the desired instability.

Taylor (1923) first observed the instability of fluid when the inner cylinder exceeds a critical speed between two coaxial cylinders in his established work. The laminar flow confined within the annulus region between two coaxial cylinders with the inner one differentially rotating with respect to the outer suffers centrifugal instability depending on the geometry and rotation rates. Taylor (1923) showed that an inviscid rotating flow to be

unstable, if the energy of rotation associated with fluid particle decreases radially outward. Under such unstable configuration, one notices the appearance of circumferential toroidal vortices in between the two cylinders and is known as Taylor–Couette vortices. These vortices evolve due to the adverse gradient of angular momentum that creates potential unstable arrangement of flow. Such an unstable condition arises naturally if the outer cylinder is held stationary while the inner cylinder is rotated at a sufficiently high rotation rate. In such an unstable condition, the annulus is filled with pair of counter rotating vortices. Subsequently, significant research works have been published on the hydrodynamics, transport properties, and applications of Taylor–Couette flow. Researchers analyzed the Taylor–Couette vortex flow experimentally, mathematically, and by numerical simulation and reported different flow patterns at different speed, shape and size of vortices, role of Taylor vortex on radial mixing, effect of axial flow and axial dispersion in Taylor vortex flow, contribution of Taylor vortices in heat and mass transfer, and so on.

Computer simulation was performed to observe the flow pattern within the annular space for the same reactor configuration used in our experimental study. In computing, the flow of the three-dimensional Navier–Stokes equation was solved in primitive formulation by using the commercial computational fluid dynamics (CFD) software Fluent®. *Time accurate* solution was obtained by solving the governing equations in which no simplification was made regarding symmetry and reflection of the solution. Fluent preprocessor GAMBIT® was used to create geometry and generate grid. The computation of Navier–Stokes equation for Taylor–Couette geometry is expensive. The problem was solved in a mainframe supercomputer (SGI origin 2000). The details of the computational details of simulation runs were reported elsewhere (Sengupta et al., 2001). Figure 9 shows computer-simulated results of the vortex formation and flow patterns in the annular gap between the two coaxial cylinders where the inner cylinder rotates above the critical speed. The boundary layer oscillates periodically between almost zero thickness to a maxima in between the counter-rotating vortex pair, where the two shear layers approaching each other spews out a jet of fluid toward the outer wall. The fluid particles in their motion around the toroidal vortices come periodically in contact with the inner surface where the catalyst is immobilized, and in the presence of light the catalyst is activated and as a result the redox reaction takes place. The residence time in the illuminated region is thus a function of the angular velocity of the recirculating vortex as well as the size of the vortex. The latter, once again depends on the gap size and the number of vortices formed in a given length of the reactor. The critical speed of the inner cylinder at the onset of the Taylor instability depends upon the aspect ratio (ratio of length and the annular gap) and the kinematic viscosity of fluid. If the inner cylinder speed is increased further, the flow system

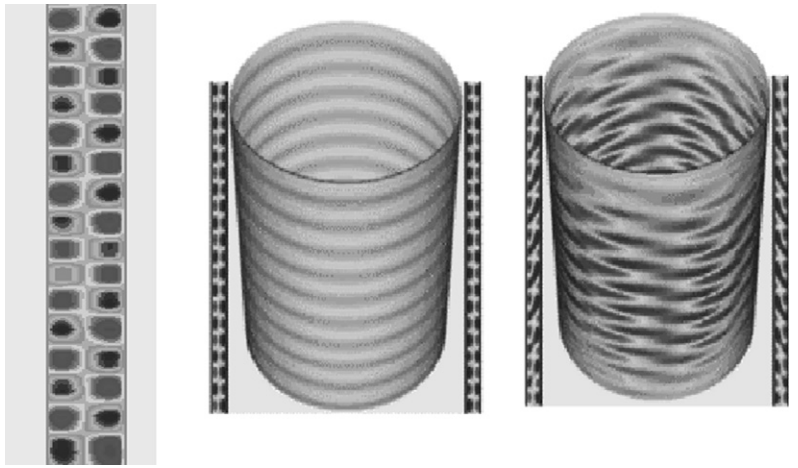

Figure 9 Flow configuration of Taylor vortices in the annular gap and contours of axial velocity in the annular space from simulation for vertical and cylindrical sections of Taylor-Couette ($Re = 177$) and wavy vortex flow ($Re = 505$) (Dutta and Ray, 2004).

exhibits a sequence of time-dependent stable vortex flow regimes as well as complicated patterns in the wide transition region between the laminar Couette flow and the turbulent vortex flow (TVF). Kataoka (1986) observed different flow patterns at different rotation speed and reported flow regions as laminar Taylor vortex flow (LTVF), singly periodic wavy vortex flow (SPWVF), doubly periodic wavy flow (DPWF), weakly turbulent wavy vortex flow (WTWVF), and TVF. The size and number of the vortices formed depended on the aspect ratio of the cylinder. However, the situation can be different for very short or infinitely long cylinder. Moreover, the effective wavelength depends on the initial and boundary conditions. This has been attributed to the existence of many stable solutions of the governing Navier–Stokes equation for flows far from equilibrium. Coles (1965) investigated systematically the wavy vortex flow and found that there are several distinct stable flow states depending upon the path through which final (steady state) Reynolds number is reached. This suggests nonuniqueness of the flow pattern or the possibility of existence of multiple solutions. Rayleigh (1920) was first to deduce the criteria of centrifugal instability where he stated that an inviscid rotating flow is unstable if the energy of the rotating fluid particles decreases radially outward. An unstable condition arises when the outer cylinder is held at stationary and the inner cylinder is rotated, the fluid near the inner cylinder experiences a centrifugal force while the fluid in the outer cylinder experiences the presence of stationary wall. If the rotation is increased further, the centrifugal force overcomes the stabilizing viscous flow and these two opposing forces create

instability by creating series of pair of counter rotating vortices where the diameter of an individual vortex is approximately equal to the annular gap. In other words, stability is ensured if

$$\frac{\mathrm{d}}{\mathrm{d}r}[rv_\theta]^2 > 0 \tag{5}$$

According to Taylor (1923), the flow instability is observed when the Taylor number exceeds a critical value where Taylor number is defined by geometrical parameters and the speed of rotation:

$$Ta = Re^2\left[\frac{d}{r_i}\right] \tag{6}$$

where $Re = r_i\omega d/v$.

Sczechowski et al. (1995) was the first to study experimentally Taylor–Couette flow instability in photocatalytic reactor to enhance the photoefficiency. They observed that when catalyst particles were used as suspension, the useful reaction took place only periodically. Taylor–Couette flow allows catalyst particles to get into the continuous periodic illumination since only part of the reactor is illuminated due to optical dense fluid. Vortices created in Taylor–Couette flow move the catalyst particles into and out of the illumination area and thus allow pollutants to come into periodic contact with light and darkness. The residence time of the particles in the illuminated area is thus a function of the angular velocity of the recirculating vortices as well as the size of the vortex. They observed 30% higher photoefficiency at 300 rpm by using an unusually high catalyst loading of 10 g L^{-1}. However, slurry system raises the question of separating the submicron-size catalyst particles after degradation of pollutants. In addition, photoefficiency can only be increased at higher rotation speed and at unusual higher catalyst loading, which might not be feasible in practical application. Based on the above considerations, our research group has designed a new Taylor Vortex photocatalytic Reactor (TVR) where the outer surface of the inner cylinder is coated with catalyst and the fluorescent lamp is placed inside of the inner cylinder. The immobilization of catalyst eliminates the need for separation of submicron-size particles after treatment.

3.4. Experimental details

3.4.1. The reactors

Figure 10 shows schematic drawing of the novel bench-scale reactor system based on hollow tubes. The reactor (MTR) consists of a cylindrical vessel of diameter 0.056 m within which 54 hollow quartz glass tubes of diameter 0.006 m coated on its peripheral surface with catalyst were placed. The tubes were held securely within the reactor by two teflon end plates on which

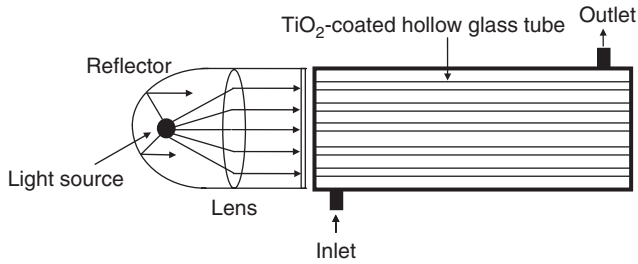

Figure 10 Schematic diagram of multiple tube reactor (MTR) (Ray, 1999).

54 holes were drilled. The reactor resembles that of a shell- and tube-heat exchanger with reaction liquid flowing through the shell-side over the outside surfaces of the coated tubes while light travels through the inside of hollow tubes. The tubes were arranged in triangular pitch of 0.007 m, thereby achieving a very high surface area per unit volume. The feed was introduced through four equally distributed ports at one end of the vessel, thereby minimizing formation of any dead zones. Similarly, the exit flow from the reactor was collected through four ports distributed at the other end of the reactor. One end of each tube was closed to prevent any reaction liquid entering the inside of the tubes. The closed ends were also coated with aluminum for better utilization of axially exiting light. The glass material used was quartz instead of Pyrex. Although quartz is more expensive than Pyrex glass when glass slabs or rods are considered, the price difference is not so appreciable when glass test tubes are considered. The quartz was used in the setup particularly for two reasons: (a) transmission of light in Pyrex is very poor compared to quartz and therefore, the length of hollow glass tubes that can be used in the reactor will be restricted and (b) when using large number of 5–6-mm test tubes, use of quartz tubes will increase the strength of the reactor and it will be much easier to handle bundle of long but narrow diameter hollow test tubes without worrying about breakage of the tubes. Of course, if one uses Pyrex tubes, reactor will be cheaper but then the length of the reactor has to be reduced. The light source (Philips GBF 6436, 12 V, 40 W) used in MTR was a low-voltage halogen lamp optically positioned in a lightweight highly glossy anodized aluminium reflector spanning 0.056 m for a clearly defined beam spread. In addition, a condenser lens of focal length 0.04 m was placed between the lamp and the reactor to obtain light beam at a half intensity beam angle between 2 and 4°.

The TLR (Figure 11) consists of a stainless steel flat top plate (0.132×0.016 m) with 21 holes onto which another plate (0.248×0.132 m) was welded. Twenty-one U-shaped lamps were placed around the latter plate and its end extended through the holes for electrical connections.

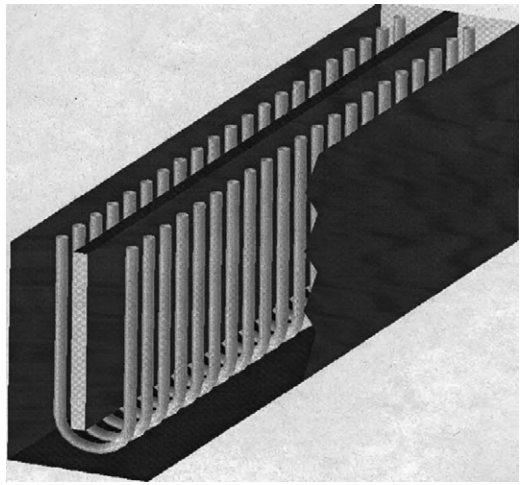

Figure 11 Schematic diagram of tube light reactor (TLR) (Ray and Beenackers, 1998).

Electrical wires were connected to the novel lamps through copper holders that are screwed around the lamp end. This part acts as a clamp for the lamps. The assembly was put in a rectangular stainless steel reactor vessel. Feed is introduced at the top of the vessel and is equally distributed over the width of the reactor through five inlet ports thereby minimizing formation of any dead zones. Similarly, the flow exits the reactor through five ports at the other end. The effective illuminated surface areas of the catalyst and the volume of the reactor are $0.15\,m^2$ and $5.36 \times 10^{-4}\,m^3$, respectively. The parameter κ, defined as total illuminated catalyst surface area that is in contact with reaction liquid per unit volume of liquid treated in the reactor volume, is equal to $618\,m^2\,m^{-3}$. The novel lamps (Philips NDF-U2 49-6W) used in TLR were specially developed by Philips Lighting for our experiments. The U-shaped lamps are 0.498 m long and have a diameter of 0.0045 m only. These operate at 1020 V, produce 6 W of which 15% is in the UV-A region. The light intensity ($\lambda < 380\,nm$) on catalyst particles is $127.8\,W\,m^{-2}$.

In Figure 12, a schematic view of the Taylor Vortex Reactor (TVR) used is shown, which consists of two coaxial cylinders (with $r_i/r_o = 0.796$ and aspect ratio, $L/d = 38.24$) made of Perspex in which the inner one rotates while the outer one remains stationary. Perspex is used as it makes it easy for handling, and moreover, it can cut off light in UV-B and UV-C ranges and thereby eliminates direct photolysis of organic compounds. The catalyst was coated on the outer surface of the inner cylinder, which can be rotated at variable speed achieved through gear coupling, a stepper motor together with a frequency generator. A UV lamp (Philips, TLK 40W/10R) was mounted inside of the inner cylinder. The lamp has a spectral distribution

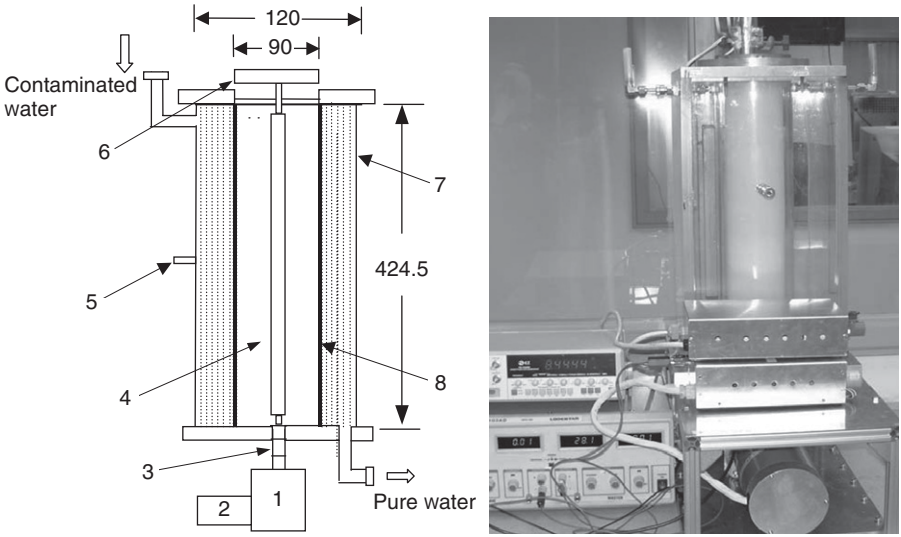

Figure 12 Experimental set-up of Taylor vortex photocatalytic reactor (Dutta and Ray, 2004): (1) motor, (2) speed controller, (3) gear coupling, (4) UV lamp, (5) sample collection point, (6) lamp holder, (7) outer cylinder, (8) catalyst-coated inner cylinder.

energy with a sharp (primary) peak at $\lambda = 365\,\text{nm}$ with an incident light intensity $13\,\text{W}\,\text{m}^{-2}$. The volume of the annular region (in which the reaction liquid is present) is equal to 1.45 L and the reactor was operated in batch mode. A sampling port was made near the middle portion of the reactor through which samples were collected by a syringe. A UV radiometer (Cole-Parmer Instrument Series 9811) was used to measure the intensity of the light around 365 nm wavelength. The rpm of inner cylinder was determined with a tachometer.

3.4.2. Catalyst

Degussa P25 grade TiO_2 was used as catalyst for all the experiments. The crystalline product is nonporous primarily in the anatase form (70:30 anatase to rutile) and is used without further treatment. It has a BET surface area of $(5.5 \pm 1.5) \times 10^4\,\text{m}^2\,\text{kg}^{-1}$ and crystallite sizes of 30 nm in 0.1–0.3 μm diameter aggregates.

3.4.3. Catalyst immobilization

For better catalyst fixation and its durability, the glass surface of the tubes and the lamps on which titania was deposited were roughened by sand blasting. This makes the catalyst surface uneven but increases the strength and amount of catalyst per unit area that could be deposited. It is known that adherence of TiO_2 on quartz is poor than on Pyrex. However, when the

glass surface was roughened, the adherence improved appreciably. The glass surface was carefully degreased, cleaned with 5% HNO_3 solution overnight, washed with water, and then dried. A 5% aqueous suspension of the catalyst was prepared with water out of Millipore Milli-Q water purification system. The suspension was mixed in an ultrasonic cleaner (Branson 2200) bath to obtain a milky suspension that remained stable for weeks. The lamp's surfaces were coated with catalyst by dip-coating apparatus designed for coating catalyst. This is completely automated equipment capable of immobilizing catalyst onto a variety of different shaped and sized substrates to any desired thickness by successive dipping of the objects into a suspension at controlled speed that can be varied between 0.4 and $4.0 \times 10^{-4}\,\mathrm{m\,s^{-1}}$. Four 250-W infrared lamps were attached to a clamp that can be moved both vertically and horizontally for instant drying of the coating. After coating, it was dried and then fired at a temperature of 300°C. Catalyst coating thus obtained on a roughened glass surface was very stable. Hardly any catalyst washes away under running water. In addition, roughening of glass surface helped in achieving better light distribution due to reduction in total internal reflection of light.

3.4.4. Model component and analysis

Laboratory grade Orange II (Acid orange 7, MW 350.3, dye content 85%) was used as model component. This is an excellent model component for the characterization of a photocatalytic reactor as the dye is reactive only in presence of both TiO_2 and UV light and biologically not degradable. Changes in Orange II concentration were measured using Shimadzu UV-1601PC UV-Visible-Spectrophotometer at wavelength of 485 nm. A shimadzu 5000A total organic carbon (TOC) analyzer with an ASI-5000 autosampler was used to analyze the TOC for the model compounds.

3.4.5. Experimental setup

A gear pump (Verder model 2036) was used for pumping the reactant between the reactor and the reservoir via a flow-through cuvet placed inside a universal photometer (Vitatron 6000) for continuous on-line measurement of the model component (Figure 13). Two three-way glass valves were used between the water and specially designed reactant reservoir for initial zero setting of the analytical instrument before the start of an experiment, introduction of the reactant into the system, elimination of bubbles formed during experiment, and final flushing of the entire system.

3.4.6. Experimental procedure

At the start of every experiment, the reactor was rinsed with Milli-Q water before zero-setting the analytical instrument. The reactor was then filled with the dye solution and it was ensured that no air bubbles remained in the system. The change in the dye concentration was continuously recorded.

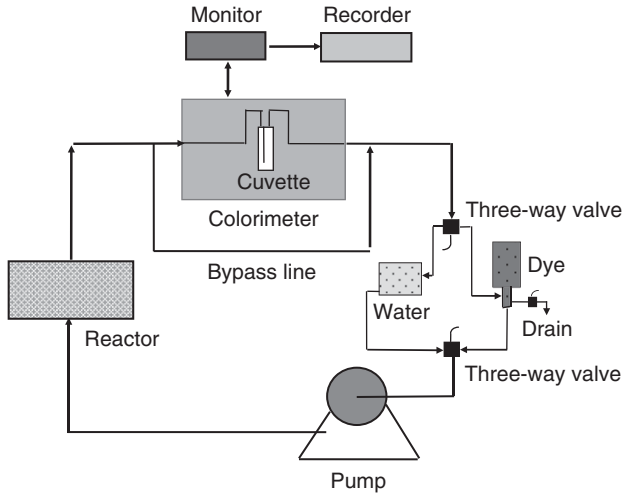

Figure 13 Experimental setup. Different reactors described in this chapter were used in the "Reactor" block.

New silicon connecting tubes and fresh catalysts were found to adsorb the dye for about an hour, but no noticeable adsorption by the entire system was observed afterward. Light was turned on only when the colorimeter reading was stabilized. For the analysis of Taylor vortex reactor, various visualization fluids (AQ-RF, AQ-1000, ST-1000, AQ-Red Dye) from Kalliroscope Corporation were used to observe the flow pattern in the annular gap for Taylor vortex reactor. AQ-RF rheoscopic fluid was used as received while AQ-1000 rheoscopic concentrate, ST-1000 bacterial stabilizer, and AQ-Red dye were mixed in required proportion to get proper visualization at different speeds. Degussa P25 grade TiO_2 was used as photocatalyst as received. The outer surface of the inner cylinder was coated with TiO_2 using a fully automated dip-coating apparatus described elsewhere (Ray and Beenackers, 1998).

Varied catalyst film thickness can be obtained by controlling the number of times coated and the speed of coating. For the Taylor vortex reactor, the experiments were carried out in two phases. In the first phase, only Taylor-Couette flow development was studied at different speeds of rotation (Reynolds number) of the inner cylinder using different flow visualization fluid. Time needed for vortex formation and its movement toward center from both ends, vortex pattern, number of vortices within the reactor length, changes of flow pattern upon increasing the speed of rotation, and the effect of mode of starting (slow or sudden increase) of rotation of the inner cylinder were recorded. In the second phase, photocatalytic degradation experiments were carried out for the three model compounds.

3.4.7. Results and discussion

The reaction rate was found out to be a function of flow rate indicating that reaction is mass transfer controlled. Experimental results reveal that 90% of the pollutant was degraded in about 100 min for MTR (Ray, 1999) and in about 30 min for TLR (Ray and Beenackers, 1998). This was achieved even though the reactor was far from optimum with respect to mass transfer, flow distribution, and efficiency of packing of the tubes in the reactor. In fact, performance of the reactor can be instantly improved by decreasing the length of the hollow tubes as it is likely that catalyst is almost inactive near the end of the 0.5 m long tube away from the light source. It is apparent that MTR design idea creates great opportunities for building much more efficient photocatalytic reactor. The main problem in the development of MTR design concept is that it is impossible to obtain uniform light distribution along the length of the tubes, and thereby, restricting the maximum length of tubes that can be used. One way of avoiding this is to place one extremely narrow diameter novel lamps inside each of the hollow tubes. In this way, all the advantages of the MTR can be retained while eliminating the basic drawback of uniform light distribution dilemma. Moreover, this will also eliminate the main problem experienced in the TLR with the prolonged use of the novel lamps in contact with reaction liquid.

Time-dependent LTVF was observed when the rotation of the inner cylinder exceeds 2.2 rpm ($Re > 111$). The vortex starts at the bottom of the cylinder at the critical Reynolds number and moves toward center of the cylinder with time. The flow was monitored using the Kalliroscope fluid (AQ 1000) and in our system, it took about 12 min to reach steady state as shown in Figure 14.

At steady state, about 21 counter rotating vortex pairs were observed and the dimension of the each counter rotating pair was almost twice the gap of the annular space. It was also observed that

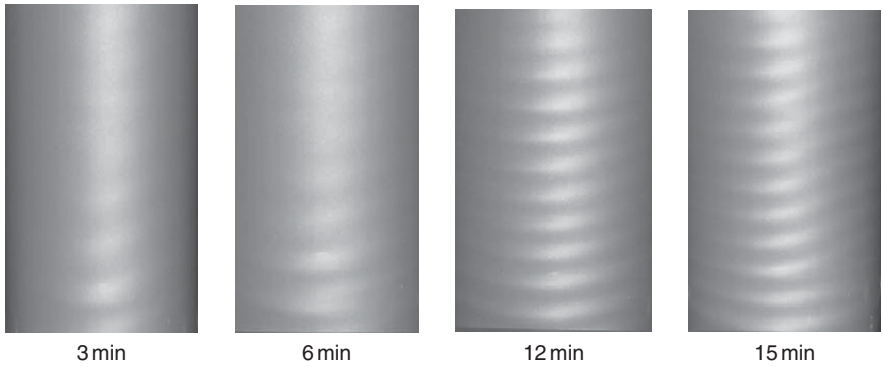

Figure 14 Progress of time-dependent Taylor vortex flow around critical Reynolds number, $Re_c = 111$. (Dutta and Ray, 2004).

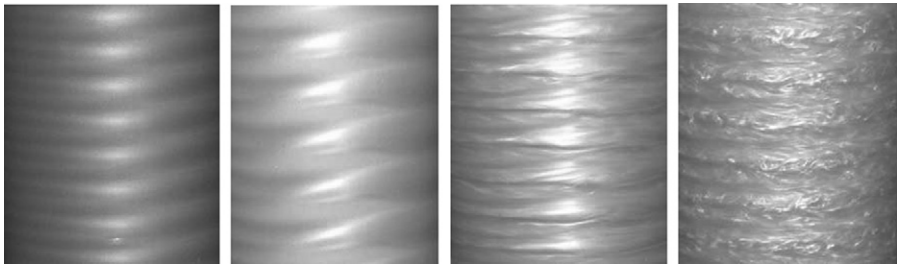

Figure 15 Photograph of flow pattern at different Reynolds number. (a) Taylor vortex flow ($Re = 177$), (b) wavy vortex flow ($Re = 505$), (c) weakly turbulent vortex flow ($Re = 3027$), and (d) turbulent vortex flow ($Re = 8072$) (Dutta and Ray, 2004).

the outflow boundary is easily distinguishable while the inflow boundary is not so easily distinguishable with bare eye at this critical Reynolds number. When the Reynolds number was increased beyond a secondary critical value of about 228 ($Re/Re_c = 2.05$), Taylor vortex flow takes the shape of azimuthally traveling waves. This wavy vortex flow exists until the Reynolds number reaches about 1,770 ($Re/Re_c \approx 16$) at which the flow transforms into turbulent flow. In the turbulent region, we observed at first weakly TVF, which changes to fully TVF at even higher Reynolds number. Figure 15 shows photographs of the flow patterns at different Reynolds number observed using the flow visualization fluid.

In Table 3, reactor specifications and experimental conditions used and efficiency obtained for the different reactors are compared. A more practical "engineering" definition for efficiency is used instead of more scientific quantum efficiency. The efficiency of each of the reactors, expressed in terms of 50% pollutant converted per unit time per unit reactor volume per unit electrical power consumed, is compared for the same model component (Orange II dye) and same initial concentration ($C_0 = 0.024\,\text{mol m}^{-3}$). The SR consists of 20 tubes each of volume $7 \times 10^{-5}\,\text{m}^3$ containing $3 \times 10^{-5}\,\text{m}^3$ of liquid (with TiO_2 concentration of $0.5\,\text{kg m}^{-3}$), placed on a holder that rotates around a magnetic stirrer and is surrounded by 24 Philips TLK 40 W/10 R lamps. The CAR was of 0.099 m outside diameter and 0.065 m inside diameter and 0.77 m long, surrounded externally with 10 Philips TLK 40 W/10 R lamps. When the efficiencies of these test reactors are compared (Table 3) with the experimental results of CAR, an increase of about 229% for SR, 1157% for MTR, 1668% for TLR, and 872% for TVR. This increase in efficiency was despite the fact that the design of these test reactors was far from optimum. In our laboratory, we have used Perspex as material (to avoid breakage), which reduces light intensity significantly. Moreover, the lamp used in this study had UV-A intensity of only $13\,\text{W m}^{-2}$,

Table 3 Comparison of reactor specifications, experimental conditions, and reactor performance efficiency for photocatalytic decomposition of Orange II dye

Photocatalytic reactor	CAR[c]	SR[c]	MTR[d]	TLR[c]	TVR[e]
Volume of reactor (m^3)	3.5×10^{-3}	3.4×10^{-3}	1.2×10^{-3}	5.4×10^{-4}	3.7×10^{-3}
Catalyst surface area (m^2)	0.18	3.7	0.51	0.15	0.12
Parameter κ (m^{-1})	69	6139[b]	1087	618	102
Flow rate ($m^3\ s^{-1}$)	8.4×10^{-5}	Batch operation	3.0×10^{-5}	1.7×10^{-5}	Batch operation
Volume of liquid treated (m^3)	2.6×10^{-3}	6.0×10^{-4}	4.7×10^{-4}	2.4×10^{-3}	1.1×10^{-3}
Electrical energy input (W)	400	960	40	126	40
Efficiency[a] ($s^{-1}\ m^{-3}\ W^{-1}$)	9.43×10^{-4}	3.1×10^{-3}	1.18×10^{-2}	1.67×10^{-2}	9.17×10^{-3}
% increase in efficiency	0	229	1157	1668	872

[a]Efficiency is defined as 50% pollutant converted per unit time per unit reactor volume per unit electrical energy used.
[b]The value will be lower than 6,139 m^{-1} as all suspended catalyst particles will not be effectively illuminated and the assumption of average particle diameter of 0.3 μm may be too low.
[c]Ray and Beenackers, 1998.
[d]Ray, 1999.
[e]Dutta and Ray 2004.

and the overall rate could be increased significantly if a higher wattage lamp is used. It is apparent that TVR design idea creates great opportunities for building much more efficient photocatalytic reactor.

Both the MTR and the TLR design concept creates great opportunities for building much more efficient photocatalytic reactors for water purification as the reactors will be more economical. From Tables 2 and 3, it can be seen that higher values for the parameter κ can be achieved for both MTR and TLR than other reactor configurations. It is expected that the performance of TLR will surpass that of MTR because of superior catalyst activation, but the overall reactor efficiency may be much lower due to the application of a large excess of light energy than is required for catalyst activation. It is apparent that MTR design idea creates great opportunities for building much more efficient photocatalytic reactor for water purification, as the reactor most likely will be economical. We believe that MTR reactor will be cost effective compared to other photocatalytic reactors since it consists of inexpensive hollow glass tubes, cheap catalyst, and requires low-wattage lamps. It needs a reflector, which usually comes with the lamp and, of course, a lens to direct the light entry at proper angle. Moreover, the hollow test tubes could easily be replaced. It is well known that water purification by photocatalysis will not be cheaper than, for example, by biotreatment. However, if one is interested in purifying water-containing toxic chemicals, the best method may be to break open the benzene ring first by photocatalysis to eliminate the toxic chemicals and then send the water for biotreatment. It would then not be necessary to completely mineralize the pollutants present in water by a photocatalytic reactor. A combination of the two methods could be best suited for water purification and may be more economical. A problem for TLR is still the burning stability and lifetime of the lamps, particularly when the lamps are used immersed in water containing toxic chemicals. The main obstacle to the development of MTR design concept is that it is impossible to obtain uniform light distribution along the length of the tubes and thereby severely restricting the maximum length of tubes that can be used. One way of avoiding both the problems is to place one extremely narrow diameter novel tubelight lamp inside each of the hollow tubes. In this way, all the advantages of the MTR concept can be utilized while eliminating the basic drawback of uniform light distribution dilemma. Moreover, this will also eliminate the main problem experienced in the TLR with the prolonged use of novel lamps immersed in polluted water.

4. CONCLUSIONS

Heterogeneous photocatalysis on semiconductor particles has been shown to be an effective means of removing toxic organic pollutants as well as toxic metal ions from water. In the first part of this chapter, systematic kinetic

studies of parameter influence (catalyst loading, circulation rate, substance initial concentration, light intensity) on the reaction rate of photocatalytic degradation of benzoic acid in TiO_2 slurry systems has been presented. Operating with the data "reaction rate versus catalyst loading," it was observed that when rate data is plotted per unit mass of catalyst, one could identify "kinetic" region from the constancy of rate data. In contrast, when the same experimental data was plotted with rate data expressed as per unit volume of reaction liquid, one could identify the region of "optimal catalyst loading" from the constancy of the rate data where rate is limited primarily by internal mass transfer due to agglomeration of catalyst particles. "Kinetic limitation" domain occurs at low catalyst loading and intrinsic (true) kinetic dependences, particularly "reaction rate – light intensity" can only be obtained from the data in the "kinetic" region. "Optimal catalyst loading" domain is a distinctive part of the "transport" limitation domain (which occurs at intermediate values of catalyst loading and is a general feature of the multiphase catalytic process) in which reaction rate is likely governed by transport processes within the catalyst particle agglomerate (estimated size of the agglomerate was found to be 9 μm), that is, internal mass transport limitation. It was observed that in the "optimal catalyst loading" region, there is no external mass transport limitation, but circulation rate influences agglomeration of catalyst particles as the rate plateau shifts toward higher value of catalyst loading when circulation rate is increased. Significant difference in the rate values between the "optimal catalyst loading" regime and the "kinetic regime" was observed. Determination of this region is very important as one can readily obtain from the "kinetic" regime the intrinsic reaction rate constant, which is required for catalyst characterization, elucidation of mechanism of the photocatalytic reaction and in the reactor design, while determination of "optimal catalyst loading" is important for practical applications. It is, however, difficult to distinctively distinguish "internal mass transfer" limitation regime and "shielding effect" domain as they are most likely overlapping. The analysis presented in the first part for slurry system can be used for any heterogeneous catalysis systems.

Several challenges related to photocatalysis and reactor designs are described in the later part of the chapter. The central problems in the development of a photocatalytic reactor, namely, light distribution inside the reactor, providing high surface areas for catalyst per unit reactor volume, and mixing inside the reactors are discussed. Several new reactor concepts, namely, a distributive-type fixed-bed reactor system that employs hollow glass tubes as a means of light delivery to the catalyst particles, an immersion-type reactor where new extremely narrow diameter artificial fluorescent lamps coated with catalyst, and a reactor based on utilization of flow instability to increase mixing, are discussed. All reactors result in a 100- to 150-fold increase in surface area per unit volume of reaction liquid

inside the reactor relative to a CAR design and a 10- to 20-fold increases relative to an immersion-type reactor using classical lamps. The design of all the reactors increases the surface-to-volume ratio while eliminating the prospect of light loss by absorption and scattering in the reaction medium. Simulation as well as experiments studies performed to understand the degradation of an Orange II dye showed promising results. All reactor configurations are flexible enough to be scaled-up for commercial applications.

ACKNOWLEDGMENTS

The author acknowledges research contributions made by research collaborators Professor Virender K. Sharma (Florida Institute of Technology), Professor Gregory Yablonsky (Washington University at St. Louis), Professor Tapan K. Sengupta (Indian Institute of Technology, Kanpur), Professor George Zhao (National University of Singapore), and graduate students (Dingwang Chen, Jinkai Zhou, Yuxin Zhang, Vidyaniwas Khetawat, Preety Mukherjee, Uvaraj Periyathamby, Mohammad Kabir, Shuhua Zhou, Kanheya Mehrotra, Xiaoling Wang, Paritam K Dutta, Yong Yong Eng, Atreyee Bhattacharya, Fengmei Li, Muthusamy Sivakumar, Debjani Mukherjee, Mahmoud Housyn, and Pankaj Chowdhury) without whom the research presented here would not be possible.

REFERENCES

Anderson, M.A., Tunesi, S., and Xu, Q. US 5035784 A 910730 (1991).

Assink, J.W., Koster, T.P.M., and Slaager, J.M. "Fotokatalytische oxydatie voor afvalwater behandeling". Internal report reference no. 93–137, TNO – Milieu en Energie, The Netherlands (1993).

Bard, A.J. *Science* **207**, 139 (1980).

Blake, D.M. "Bibliography of work on Photocatalytic Removal of Hazardous Compounds from Water and Air". NREL/TP-430-22197, National Renewable Energy Laboratory, Golden (1997).

Cassano, A., Martin, C, Brandi, R., and Alfano, O. *Ind. Eng. Chem. Res.* **34**, 2155 (1995).

Chen, D.W., Li, F., and Ray, A.K. *AIChE J.* **46**, 1034 (2000a).

Chen, D.W., Li, F., and Ray, A.K. *Catal. Today* **66**, 475 (2001).

Chen, D.W., and Ray, A.K. *Appl. Catal. B* **23**, 143 (1999).

Chen, D.W., and Ray, A.K. *Chem. Eng. Sci.* **56**, 1561 (2001).

Chen, D.W., and Ray, A.K. *Water Res.* **32**, 3233 (1998).

Chen, D.W., Sivakumar, M., and Ray, A.K. *Dev. Chem. Eng. Miner. Proces.* **8**, 505 (2000b).

Coles, D. *J. Fluid Mech.* **21**, 385 (1965).

Cooper, G.A.US patent 4888101 (1989).

Cooper, G.A., and Ratcliff, M.A.WO 9108813 A1 910627 (1991).

de Lasa, H., Serrano, B., and Salaices, M. "Photocatalytic Reaction Engineering". Springer, USA (2005).

de Lasa, H.I., and Valladares, J. US Patent No. 5, 683, 589 (1997).

Dutta, P.K., and Ray, A.K. *Chem. Eng. Sci.* **59**, 5249 (2004).

Dutta, P.K., Sharma, V., and Ray, A.K. *Environ. Sci. Technol.* **39**, 1827 (2005).

Fox, M.A., and Dulay, M.T. *Chem. Rev.* **93**, 341 (1993).

Haneda, K.Patent JP 04061933 A2 920227 (1992).
Heller, A., and Brock, J.R.Patent WO 9317971 A1 930916 (1993).
Henderson, R.B., and Robertson, M.K.Patent EP 3063301 A1 890308 (1989).
Hoffmann, M.R., Martin, S.T., Choi, W., and Bahnemann, D.W. *Chem. Rev.* **95**, 69 (1995).
Hofstadler, K., Bauer, R., Novallc, S., and Helsler, G. *Environ. Sci. Technol.* **28**, 670 (1994).
Hosokawa, M., and Yukimitsu, K.Patent JP 63042793 A2 880223 (1988).
Inel, Y., and Okte, A.N. *J. Photoch. Photobio. A.* **96**, 175 (1996).
Kataoka, K. Taylor vortices and instabilities in circular Couette flows. *in* N.P. Cheremisinoff (Ed.), "Encyclopedia of Fluid Mechanics", vol. 1. Gulf Publishing, Houston (1986), p. 236.
Masuda, R., Kawashima, K., Takahashi, W., Murabayashi, M., and Ito, K.Patent JP 06320010 A2 941122 (1994).
Matthews, R.W. Patent AU 600289 B2 900809 (1990a).
Matthews, R.W. Patent WO 8806730 A1 880907 (1998).
Matthews, R.W. *Water Res.* **24**, 663 (1990b).
Mehrotra, K., Yablonsky, G.S., and Ray, A.K. *Chemosphere* **60**, 1427 (2005).
Mehrotra, K., Yablonsky, G.S., and Ray, A.K. *Ind. Eng. Chem. Res.* **42**, 2273 (2003).
Miano, F., and Borgarello, E.Patent EP 417847 A1 910320 (1991).
Mukherjee, P.S., and Ray, A.K. *Chem. Eng. Technol.* **22**, 253 (1999).
Oonada, J.Patent JP 06071256 A2 940315 (1994).
Peill, N.J., and Hoffmann, M.R. *Environ. Sci. Technol.* **29**, 2974 (1995).
Periyathamby, U., and Ray, A.K., *Chem. Eng. Technol.* **22**, 881 (1999).
Pruden, A.L., and Ollis, D.F. *Environ. Sci. Technol.* **17**, 628 (1983).
Ray, A.K. *Catal. Today* **44**, 357 (1998).
Ray, A.K. *Des. Chem. Eng. Sci.* **54**, 3133 (1999).
Ray, A.K., and Beenackers, A.A.C.M. *AIChE J.* **43**, 2571 (1997).
Ray, A.K., and Beenackers, A.A.C.M. *AIChE J.* **44**, 477 (1998a).
Ray, A.K., and Beenackers, A.A.C.M. *Catal. Today* **40**, 73 (1998b).
Ray, A.K., and Beenackers, A.A.C.M. European patent, EP 96200942.9-2104 (1996).
Rayleigh, L. "Scientific Papers", vol. 6. Cambridge, England (1920), p. 447.
Rideh, L., Wehrer, A., Ronze, D., and Zoulalian, A. *Ind. Eng. Res.* **36**, 4712 (1997).
Ritchie, D.G. Patent US 5069885 A 911203 (1991).
Salaices, M., Serrano, B., and de Lasa, H. *Ind. Eng. Chem. Res.* 40, 5455 (2001).
Sato, K.Patent JP 04114791 A2 920415 (1992).
Sczechowski, J.G., Koval, C.A., and Noble, R.D. *Chem. Eng. Sci.* **50**, 3163 (1995).
Sengupta, T.K., Kabir, M.F., and Ray, A.K. *Ind. Eng. Chem. Res.* **40**, 5268 (2001).
Serpone, N., and Pelizetti, E. (Ed.), "Photocatalysis: Fundamentals and Application". Wiley, New York (1989).
Serrano, B., and de Lasa, H.I. *Chem. Eng. Sci.* **15**, 3063 (1999).
Serrano, B., and de Lasa, H.I. *Ind. Eng. Chem. Res.* **36**, 4705 (1997).
Taoda, H. "Water Treatment". Patent JP 05076877 A2 930330 (1993).
Taylor, G.I. *Trans. Roy. Soc. Lond. A* **223**, 289 (1923).
Wake, H., and Matsunaga, T.Patent JP 06134476 A2 940517 (1994).
Wang, X., Pehkonnen, S.O., andRay, A.K. *Electrochem. Acta* **49**, 1435 (2004a).
Wang, X., Pehkonnen, S.O., and Ray, A.K. *Ind. Eng. Chem. Res.* **43**, 1665 (2004b).
Zhou, J., Takeuchi, M., Ray, A.K., Anpo, M., and Zhao, X.S. *J. Colloid Interface Sci.* 311, 497 (2007a).
Zhou, J., Takeuchi, M., Zhao, X.S., Ray, A.K., and Apno, M. *Catal. Lett.* **106**, 67 (2006a).
Zhou, J., Zhang, Y., Zhao, X.S., and Ray, A.K. *Ind. Eng. Chem. Res.* **45**, 3503 (2006b).
Zhou, J., Zou, Z., Zhao, X.S., and Ray, A.K. *Ind. Eng. Chem. Res.* **46**, 745 (2007b).